# Modeling of argon–acetylene dusty plasma

Igor Denysenko, Eric von Wahl, Safa Labidi, Maxime Mikikian, Holger
Kersten, Titaïna Gibert, Eva Kovacevic, Nikolay A. Azarenkov

## HAL Id: hal-01978171
## https://hal.science/hal-01978171

# Modelling of argon-acetylene dusty plasma

**I.B. Denysenko[1], E. von Wahl[2,3], S. Labidi[3], M. Mikikian[3], H. Kersten[2],**

**T. Gibert[3], E. Kovačević[3] and N.A. Azarenkov[1]**

[1]School of Physics and Technology, V. N. Karazin Kharkiv National University, Kharkiv, Ukraine
[2]Institut für Experimentelle und Angewandte Physik, Universität Kiel, Kiel, Germany
[3]GREMI, UMR7344 CNRS/Université d'Orléans, F-45067 Orléans, France

E-mail: idenysenko@yahoo.com

**Abstract**

The properties of an $Ar/C_2H_2$ dusty plasma (ion, electron and neutral particle densities, effective electron temperature and dust charge) in glow and afterglow regimes are studied using a volume-averaged model and the results for the glow plasma are compared with mass spectrometry measurements. It is shown that dust particles affect essentially the properties of glow and afterglow plasmas. Due to collection of electrons and ions by dust particles, the effective electron temperature, the densities of argon ions and metastable atoms are larger in the dusty glow plasma comparing with the dust-free case, while the densities of most hydrocarbon ions and acetylene molecules are smaller. Because of a larger density of metastable argon atoms and, as a result, of the enhancement of electron generation in their collisions with acetylene molecules, the electron density in the afterglow dusty plasma can have a peak in its time-dependence. The results of numerical calculations are in a good qualitative agreement with experimental results.

# 1. Introduction

Plasmas with nano- and micrometer-sized particles (dust particles) are of a great fundamental interest and are used in many technological applications [1-4]. The dust particles can either grow inside a discharge chamber due to different chemical reactions or can be immersed into laboratory plasmas from outside. For example, formation of carbonaceous dust particles takes place in gas discharges containing methane, acetylene or ethylene [5-7].

The plasmas used for formation of carbonaceous dust particles have been intensively investigated by experimental measurements [5-11]. The measurements in $Ar/C_2H_2$ plasmas showed that formation of dust particles is accompanied by a decrease of acetylene and electron densities and by an enhancement of electron temperature and density of metastable argon atoms [11-14]. It was also found that the degree of $C_2H_2$ dissociation in an $Ar/C_2H_2$ plasma at formation of nanoparticles can be as high as 99% [13, 15]. In [13], the densities of electrons and metastable argon atoms were simultaneously measured in the glow and afterglow regimes of a pulsed radio-frequency (RF) $Ar/C_2H_2$ plasma for the dust-free and dusty plasma cases.

Properties of $C_2H_2$ and $Ar/C_2H_2$ RF plasmas were also studied by computer simulations [16-21] allowing to explain the nucleation of nanoparticles in these chemistries. In particular, it was shown that both positive and negative ions may participate as precursors in the initial stage of particle formation [17, 19]. However, most of these numerical studies considered only the initial stages of particle formation and, therefore, they did not account for effects of dust particles on plasma properties, which may be essential in some experiments. Moreover, to the best of our knowledge, the time-dependencies for densities of ions and neutral species and the effects of dust particles in the afterglow of $Ar/C_2H_2$ plasmas have not been studied yet.

In this paper, the properties of an $Ar/C_2H_2$ dusty plasma (ion, electron and neutral particle densities, electron temperature and dust charge) in the glow and afterglow regimes are studied using a global (volume-averaged) model. The effect of dust radius on the steady-state gas-discharge properties is analysed, and the properties of dust-free and dusty-plasma afterglows are compared. The results of calculations are compared with our experimental measurements on mass spectra of positive ions and neutral species in RF dust-free and dusty plasmas.

## 2. Measured mass spectra of neutral species and positive ions

In our experiment, formation of dust particles took place in a capacitively coupled asymmetric discharge running in an $Ar/C_2H_2$ mixture. The plasma discharge was driven at 13.56 MHz and a RF power of 9 W by a RF generator coupled to the bottom electrode with the help of a matching network. The grounded electrode was the entire chamber walls. The plasma height $L$ and radius $R$

were nearly 32.4 cm and 22 cm, respectively. Acetylene with the flux $Q_{C2H2}$=1.11 sccm and argon with the flux $Q_{Ar}$=10.1 sccm were used as a reactive precursor and a background gas, respectively. The process gas pressure in the reactor was about 5 Pa. The mass spectra for neutrals and positive ions were measured using the Hiden PSM 003 mass spectrometer at a height of 10 cm and a radial distance of 7 cm from the center of the powered electrode. Using this approach, we were not able to measure intensities of argon ions and neutrals at mass 40 amu simultaneously with other species because the intensity was much above saturation and the instrument would shut down.

Typical mass spectra for neutral species and positive ions, which were measured in our experiments, are shown in figures 1(a) and 1(b), respectively. The neutral mass spectrum displays that $C_2H_2$ (26 amu) is the dominant hydrocarbon neutral in the Ar/$C_2H_2$ plasma (figure 1(a)), while $H_2$ (2 amu), $C_2H$ (25 amu), $C_2H_4$ (28 amu), $H_2O$ (18 amu) and $C_4H_2$ (50 amu) are also significant neutral species. The peaks associated with argon atoms are observed at mass numbers 36 and 38 and additionally at 20 in the mass spectrum. The peaks associated with H (1 amu), CH (13 amu) and $C_6H_2$ (74 amu) are also observed. Note that the peak at mass number 28 may not be connected only with dissociation of acetylene molecules in the Ar/$C_2H_2$ plasma. It may be due to an input of $C_2H_4$ and $N_2$ in the discharge chamber [22]. The peaks of $C_2H$ and CH are mainly due to $C_2H_2$ dissociation in the mass spectrometer. Moreover, the results for H and $H_2$ should be treated very carefully as the device precision is rough for very small masses.
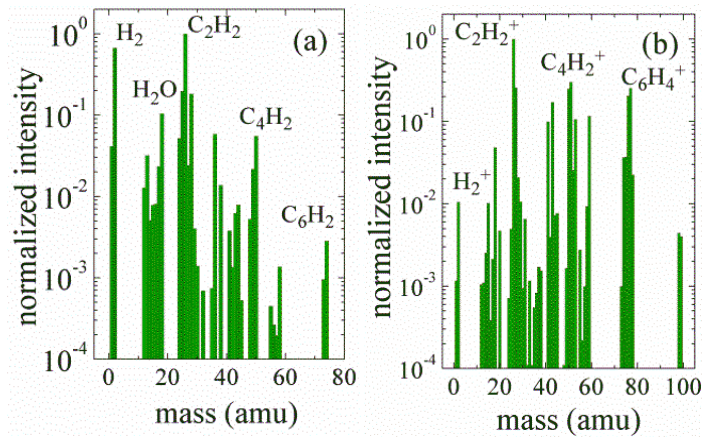


**Figure 1**. Mass spectra obtained in the Ar/$C_2H_2$ plasma for neutral species (a) and positive ions (b) for the growth phase I.

The significant ion species in the plasma are $C_2H_2^+$ (26 amu), $C_2H_3^+$ (27 amu), $C_4H_2^+$ (50 amu), $C_4H_3^+$ (51 amu), $C_6H_4^+$ (76 amu) and $C_6H_3^+$ (75 amu) (figure 1(b)). The ion peaks associated with ArH$^+$ (41 amu), $H_2^+$ (2 amu), and H$^+$ (1 amu) are about 10, $10^2$ and $10^3$ times smaller than the peak of $C_2H_2^+$.

After plasma ignition and under particular plasma conditions, the discharge displays a periodic behaviour. The temporal variation of, e.g. self-bias voltage $V_b$ and the mass peaks of neutral species, is induced by the formation of carbonaceous nanoparticles. Figure 2 shows the simultaneously measured time dependency of $V_b$ and the mass peaks of $C_2H_2$, $H_2$ and $C_4H_2$. Performing *ex situ* SEM measurements [23], we obtained information about the nanoparticle size in different growth phases. It was found that the measurable diameter of most dust particles is, respectively, in the range of 20 to 40 nm, 40 to 50 nm and 50 to 140 nm for the growth phases I, II and III.

Dust particles do not modify plasma properties during phase I (as $V_b$ stays rather constant) because of their small size. This phase has to be considered carefully as it also follows phase III of the previous cycle and could be impacted by previous dust generations. During phase II, growing nanoparticles strongly disturb the plasma as seen on $V_b$ and it corresponds to a decrease of hydrocarbon molecule signals. During phase III, these signals start increasing while nanoparticles are still growing because other dust particles possibly start to leave the discharge during phase III.
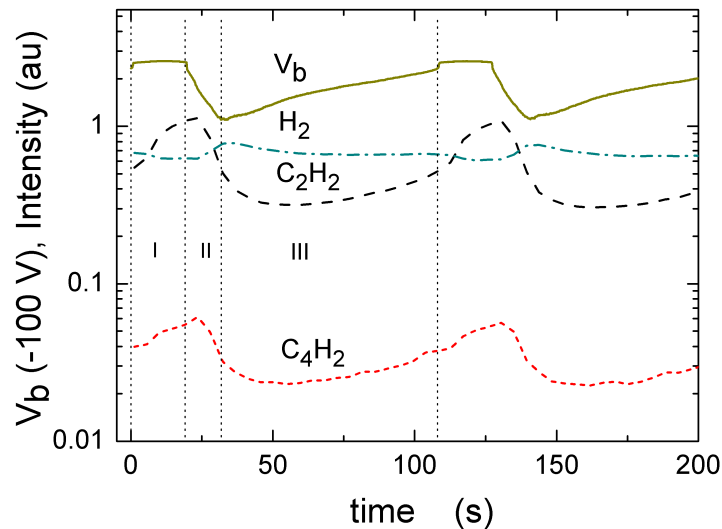


**Figure 2**. Time evolution of the self-bias voltage $V_b$ and the mass peaks of $C_2H_2$, $H_2$ and $C_4H_2$ during a growth cycle. Here, the time $t$=0 corresponds to the time 2435 s from the plasma ignition.

## 3. The volume averaged model

The properties of the $Ar/C_2H_2$ dusty plasma were analysed using a volume-averaged model. In the model, the gas-discharge plasma is sustained in a cylindrical stainless steel chamber of the same dimensions as given in the above described experiment. It is assumed that the discharge consists of electrons with density $n_e$, nine positive ions ($C_2H_2^+$, $Ar^+$, $ArH^+$, $H_2^+$, $H^+$, $C_4H_3^+$, $C_4H_2^+$, $C_6H_4^+$ and $C_2H_3^+$), four nonradical neutrals (Ar, $C_2H_2$, $H_2$, $C_4H_2$) and two radicals ($C_2H$ and H),

negatively charged dust particles with density $n_d$, radius $a_d$ (in the range of 10-70 nm) and charge $Z_d$ (in units of electron charge $e$), metastable argon atoms ($Ar_m$) with density $n_m$, argon atoms in the resonance 4s states ($^3P_1$ and $^1P_1$) ($Ar_r$) with density $n_r$ as well as argon atoms in 4p states (Ar(4p)) with density $n_{4p}$. In our model, the metastable and resonance atom densities $n_m$, $n_r$ and $n_{4p}$ represent the density of a composite $^3P_0$ and $^3P_2$ metastable level, $^3P_1$ and $^1P_1$ resonance level and 4p state, respectively. We also assume that the plasma contains negative ions $C_2H^-$ with density $n^-$, which is essentially larger than the densities of other anions. The latter assumption is applicable at large ratio of the argon input flux to the flux of acetylene [19-21].

It is assumed that the electron energy probability function (EEPF) $F$ has a Druyvesteyn shape [24]. This is typical for RF plasmas with not very large electron density and sustained in large discharge chambers or at high gas pressures [25]. For example, in the case of an argon plasma driven by a RF generator of 13.56 MHz frequency, the conditions $n_e < 10^{11}$ cm$^{-3}$ and $PL > 0.2$ Torr×cm, where $P$ is the total gas pressure, should be fulfilled. Note that in the case when the ratio of $C_2H_2$ density to that of argon atoms in the power-on phase is small, the acetylene molecules do not affect much on the EEPF shape [20].

In the model, the ions and dust particles are assumed to be at gas temperature $T_g$ (300 K). The dominant neutral species are argon atoms and their density $n_{Ar} \approx P/(k_B T_g)$, where $P = 5$ Pa and $k_B$ is the Boltzmann constant.

We assume that the plasma is quasineutral, or

$$\sum_\alpha n_\alpha^+ = n_e + n^- + |Z_d| n_d , \qquad (1)$$

where $n_\alpha^+$ is the density of $\alpha$-th positive ions.

The density of a species $X$ (ions or neutrals) is found from the balance equation

$$\frac{\partial n^{(X)}}{\partial t} = \sum_i R_{G,i}^{(X)} - \sum_i R_{L,i}^{(X)} , \qquad (2)$$

where $R_{G,i}^{(X)}$ and $R_{L,i}^{(X)}$ are, respectively, the rates for reactions describing various generation and loss processes of the species $X$ and $t$ is the time. In this study, we consider various processes for the loss and generation of the discharge species, including the collisional processes in the bulk plasma, the processes on plasma walls and dust particles, as well as the pumping of gas in and out of the chamber. The main electron-molecule (atom) processes taken into account in the model are presented in table 1. Their collision rates were calculated using the reaction cross sections given

in the references of table 1 and assuming that the EEPF has a Druyvesteyn shape. For the reactions of electrons with $C_4H_2$, the cross sections of ionization, dissociation and electron attachment are taken to be the same as those for $C_2H_2$, since no data are available in the literature. The cross sections describing the loss of $C_2H$ in collisions with electrons are taken from [26]. The reactions with participation of negative ions and their rates are shown in table 2.

We also accounted for 3 reactions between hydrocarbon neutrals ($C_2H + C_2H_2 \rightarrow C_4H_2 + H$, $C_2H + C_4H_2 \rightarrow C_6H_2 + H$, $C_2H + C_4H_2 \rightarrow C_6H_2{}^* + H$ ) and for 4 reactions between $H/H_2$ and hydrocarbon neutral species ($H + C_2H \rightarrow C_2H_2$, $H + C_2H_2 \rightarrow C_2H_3$, $H + C_4H_2 \rightarrow C_4H_3$, $H_2 + C_2H \rightarrow C_2H_2 + H$), those reaction rates are taken from [17, 18]. The reactions for collisions of excited argon atoms with various neutral species and their rates are presented in table 3.

**Table 1.** Reactions for the main electron-molecule (atom) processes taken into account in the model.

| *Reactions between electrons and argon atoms* [27-30] | |
|---|---|
| $e^- + Ar \rightarrow Ar^+ + 2e^-$ | $e^- + Ar_m \rightarrow Ar(4p) + e^-$ |
| $e^- + Ar_m \rightarrow Ar^+ + 2e^-$ | $e^- + Ar_m \rightarrow Ar_r + e^-$ |
| $e^- + Ar_r \rightarrow Ar^+ + 2e^-$ | $e^- + Ar_r \rightarrow Ar_m + e^-$ |
| $e^- + Ar(4p) \rightarrow Ar^+ + 2e^-$ | $e^- + Ar_r \rightarrow Ar(4p) + e^-$ |
| $e^- + Ar \rightarrow Ar_m + e^-$ | $e^- + Ar_m \rightarrow Ar + e^-$ |
| $e^- + Ar \rightarrow Ar_r + e^-$ | $e^- + Ar_r \rightarrow Ar + e^-$ |
| $e^- + Ar \rightarrow Ar(4p) + e^-$ | $e^- + Ar(4p) \rightarrow Ar + e^-$ |
| *Reactions between electrons and hydrocarbons* [26, 31] | |
| $e^- + C_2H_2 \rightarrow C_2H_2{}^+ + 2e^-$ | $e^- + C_2H_2 \rightarrow C_2 + 2H + e^-$ |
| $e^- + C_2H_2 \rightarrow H^+ + C_2H + e^-$ | $e^- + C_2H_2 \rightarrow C_2H^+ + H + 2e^-$ |
| $e^- + C_2H_2 \rightarrow C_2H^- + H$ | $e^- + C_2H_2 \rightarrow C_2 + H_2 + e^-$ |
| $e^- + C_2H_2 \rightarrow C_2H + H + e^-$ | $e^- + C_2H_2 \rightarrow C_2{}^+ + H_2 + 2e^-$ |
| *Reactions between electrons and $H/H_2$* [32, 33] | |
| $e^- + H_2 \rightarrow 2H + e^-$ | $e^- + H_2 \rightarrow H^+ + H + 2e^-$ |
| $e^- + H_2 \rightarrow H_2{}^+ + 2e^-$ | $e^- + H \rightarrow H^+ + 2e^-$ |

**Table 2.** Reactions with participation of negative ions.

| Reaction | Rate constant ($cm^3/s$) | Reference |
|---|---|---|
| $C_2H^- + H_2{}^+ \rightarrow C_2H + 2H$ | $1.7 \times 10^{-7}$ | [17] |
| $C_2H^- + H^+ \rightarrow C_2H + H$ | $3.0 \times 10^{-8}$ | [18] |
| $C_2H^- + ArH^+ \rightarrow C_2H + H + Ar$ | $3.0 \times 10^{-8}$ | |
| $C_2H^- + C_2H_2 \rightarrow C_4H^- + H_2$ | $1.0 \times 10^{-12}$ | [18] |
| $C_2H^- + C_mH_n{}^+ \rightarrow C_2H + C_mH_n$ | $5.0 \times 10^{-8}$ | [18] |
| $C_2H^- + Ar^+ \rightarrow C_2H + Ar$ | $1.01 \times 10^{-7}$ | [20] |
| $C_2H^- + H \rightarrow C_2H_2 + e^-$ | $1.6 \times 10^{-9}$ | [34] |

It is also accounted for 6 reactions between $Ar^+/ArH^+$ and neutral species [20, 35, 36], 29 reactions between hydrocarbon ions and neutral species [18, 37-44] and 7 reactions between $H_2{}^+/H^+$ and neutrals [18, 36, 37, 40].

The rates describing the pumping gas in and out of the chamber were calculated in the same way as in [45]. The rate describing the radical loss due to diffusion to the walls is taken as in [46, 47]. For the radical neutrals and excited argon atoms, it is also accounted for their deposition on dust particles. The sticking coefficients for $C_2H$, H and excited argon atoms are assumed to be 0.9, 0.1 and 1.0, respectively [17, 48, 49]. The amount of hydrogen incorporated into the walls and dust particles due to their interaction with $C_2H$ and H radical neutrals is set to 30%, the other amount of atomic hydrogen flows back into the plasma as molecular hydrogen gas [50]. The rates describing the positive ion loss on dust particles are calculated using the orbit-motion-limited theory [1], accounting for the ion-neutral collisions in the sheath of the dust particle [51]. We do not account for negative ion loss on dust particles and the walls because their energy is assumed to be essentially smaller than the potentials of the walls and the dust surface.

**Table 3.** Reactions with participation of argon atoms in excited states. Here, Ar* denotes argon atoms in various excited states including the metastable and 4s and 4p resonance states.

| Reaction | Rate constant ($cm^3$/s) | Reference |
|---|---|---|
| $Ar^* + C_2H_2 \rightarrow C_2H_2^+ + Ar + e^-$ | $1.8 \times 10^{-10}$ | |
| $Ar^* + C_2H_2 \rightarrow C_2H + Ar + H$ | $3.5 \times 10^{-10}$ | |
| $Ar^* + C_4H_2 \rightarrow C_4H_2^+ + Ar + e^-$ | $1.8 \times 10^{-10}$ | |
| $Ar^* + C_4H_2 \rightarrow C_4H + Ar + H$ | $3.5 \times 10^{-10}$ | |
| $Ar^* + H_2 \rightarrow ArH^* + H$ | $1.1 \times 10^{-10}$ | [35] |
| $Ar_m + Ar_m \rightarrow Ar + Ar^+ + e^-$ | $6.2 \times 10^{-10}$ | [52] |
| $Ar_m + Ar_m \rightarrow 2Ar$ | $2.0 \times 10^{-7}$ | [37] |
| $Ar_m + Ar_r \rightarrow Ar + Ar^+ + e^-$ | $2.1 \times 10^{-9}$ | [37] |
| $Ar(4p) + Ar(4p) \rightarrow Ar^+ + Ar + e^-$ | $5.0 \times 10^{-10}$ | [37] |
| $Ar_m + Ar \rightarrow 2Ar$ | $2.1 \times 10^{-15}$ | [37] |
| $Ar_r \rightarrow Ar + \hbar\omega$ | $10^5$ $s^{-1}$ | [37] |
| $Ar(4p) \rightarrow Ar + \hbar\omega$ | $3.2 \times 10^7$ $s^{-1}$ | [37] |
| $Ar(4p) \rightarrow Ar_m + \hbar\omega$ | $3.0 \times 10^7$ $s^{-1}$ | [37] |
| $Ar(4p) \rightarrow Ar_r + \hbar\omega$ | $3.0 \times 10^7$ $s^{-1}$ | [37] |

The ion mobility and ion diffusion coefficients were calculated in the same manner as in [53], while the expression for the rate describing the loss of a positive ion on the walls is taken from [46].

The next equation of our model for the steady-state case is the power balance equation

$$P_{abs} = P_{coll} + P_w + P_d, \tag{3}$$

where $P_{abs}$ is the absorbed power (in the experiment, $P_{abs} = 9$ W), $P_{coll}$ and $P_w$ are the power loss due to elastic and inelastic collisions and the loss due to charged particle fluxes to the walls, respectively [46]. $P_d$ is the power loss on the dust [54]. In calculating the power loss in collisional

processes, we accounted for the loss in collisions of electrons with $C_2H_2$, $C_4H_2$, $H_2$ and Ar with cross sections from [55-58].

The dust charge $Z_d$ is obtained from the following equation

$$\frac{\partial |Z_d|}{\partial t} = K_d^e n_e - \sum_\alpha K_d^\alpha n_\alpha^+, \tag{4}$$

where the rates $K_d^e$ and $K_d^\alpha$ describe, respectively, collection of electrons and positive ions of sort $\alpha$ by dust particles. The expressions for these rates can be found elsewhere [52, 59].

Considering the afterglow case, we assume that the effective electron temperature decays exponentially according to $T_e(t) = T_{e0} \exp(-t/\tau_T)$ with the decay time $\tau_T = 50$ μs, like in [52] and $T_{e0}$ the temperature in the power-on phase. We also assume that due to the production of energetic electrons in metastable–metastable collisions, super-elastic electron–metastable collisions and emission processes, the electron temperature cannot be smaller than 0.1 eV, i.e. after its decay to reach 0.1 eV, $T_e$ becomes time-independent.

For the steady-state case, the balance equations for $C_2H_2$, $H_2$ and H and equation (3) were solved by the iteration method (assuming $d/dt = 0$) simultaneously with the balance equations for other species and equation (4), which were solved by the 4-th order Runge-Kutta method. Applying the Runge-Kutta method, the system of first order differential equations was allowed to reach a steady state, i.e. $d/dt = 0$.

For the afterglow case, the balance equations for different species and dust charge were solved by the 4-th order Runge-Kutta method, using the initial values obtained in the steady-state calculations.

## 4. The results of calculations

### 4.1 Effects of variation of dust radius on the steady-state plasma properties

Using the theoretical model presented in section 3, we have analysed how dust particles affect the densities of various ions and neutral species in the Ar/$C_2H_2$ glow plasma. In our calculations, we varied $a_d$, while other external parameters including $n_d$, were fixed.

For the glow plasma, we assumed that the plasma is stationary because the density variation of various species due to dust growth [9, 23] is usually longer than the variations due to various collisional processes and diffusion to the walls.

The dust charge magnitude increases with increasing $a_d$ because of the increase of the dust surface collecting electrons and because of the increase of $T_e$, while $n_e$ decreases [60]. For $a_d = 10$,

20, 40, 60 nm, $n_e$ =1.82×10$^9$, 1.25×10$^9$, 4.34×10$^8$ and 1.76×10$^8$ cm$^{-3}$ and $Z_d$ = -36, -68, -113 and -130 respectively, for the conditions of figure 3. In figure 3, the calculated densities of neutral species and ions as functions of dust radius are shown. One can see in figure 3(a) that $C_2H_2$ and $H_2$ are the dominant molecules in the gas discharge, in agreement with our experimental measurements (figure 1(a)).

For the dust-free case ($a_d$=0), the argon atom density ($n_{Ar}$ ≈ 1.21×10$^{15}$ cm$^{-3}$ for P ~ 5 Pa) is 453 times larger than the density of $C_2H_2$ ($n_{C2H2}$ ≈ 2.67×10$^{12}$ cm$^{-3}$) and the degree of dissociation of $C_2H_2$ in the plasma is nearly 98 %. This agrees well with the degree estimations in [15] showing that it is in the range of 95%-99% at formation of nanoparticles.
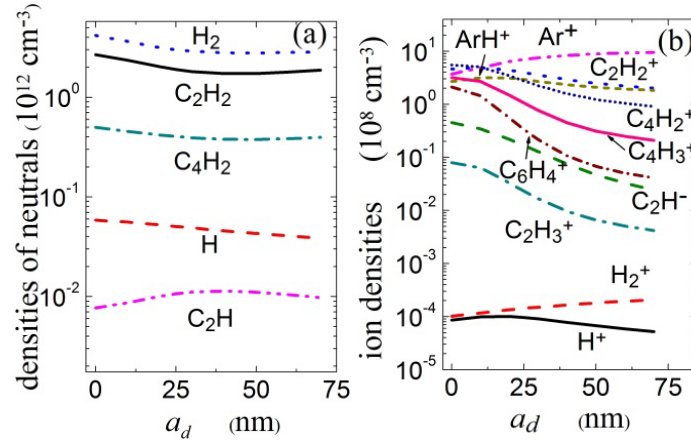


**Figure 3**. Calculated densities of neutral species (a) and ions (b) as functions of dust radius. The results are obtained for $P_{abs}$ = 9 W, $n_d$ =10$^7$ cm$^{-3}$, $Q_{C2H2}$ =1.11 sccm and $Q_{Ar}$ = 10.1 sccm.

The loss of $C_2H_2$ molecules in the plasma is mainly due to their collisions with metastable atoms, positive ions, $C_2H$ radicals and electrons. For the case of small particles ($a_d \leq$ 40 nm) the density of acetylene molecules decreases with growing particle radius (figure 3(a)) as this is accompanied by an increase of the densities of argon ions and metastable atoms, $C_2H$ radicals and by an increase of the effective electron temperature. For the case of bigger particles ($a_d \geq$ 50 nm), however, the $C_2H_2$ density slightly increases with an increase of $a_d$ because of the $n_e$ reduction. The $C_4H_2$ and $H_2$ production is related to the $C_2H_2$ density [11], and, as a result, the $a_d$ - dependencies for the $C_4H_2$ and $H_2$ densities are similar to that for $n_{C2H2}$. The decrease of H density at larger dust radius is due to higher losses of hydrogen atoms on dust particles and to a decrease of the densities of nonradical molecules and electrons, whose collisions affect the radical production. Since the main production process of $C_2H$ are the collisions of excited argon atoms with acetylene molecules and $C_2H$ is predominantly lost in the collisions with $C_2H_2$, the dependence of $C_2H$ on $a_d$ is determined mainly by the $a_d$-dependencies for densities of excited argon atoms ($n_m$ is presented in figure 4) and acetylene molecules (figure 3).

The results of calculations are in a good qualitative agreement with the experimental results revealing that the densities of $C_2H_2$ and $C_4H_2$ are decreasing with increasing the time (the dust radius) during phase II and the beginning of phase III (figure 2). However, there is a discrepancy between the simulation results and experimental data. In particular, the measured density of $H_2$ is smaller than the one of acetylene molecules during phases I and II while it's always larger in the model. The discrepancy may be due to the simplifications introduced in the 0D model. For example, our global model does not account for the spatial inhomogeneity of the plasma, while the spatial distributions of ions, radicals and dust particles are usually essentially inhomogeneous in $Ar/C_2H_2$, $C_2H_2$ and dusty plasmas [17, 20, 61]. We also do not account for the variation of neutral gas temperature during the growth cycle [62].

The dominant ions in the dust-free plasma are $Ar^+$, $C_2H_2^+$, $C_4H_2^+$, $C_4H_3^+$, $C_6H_4^+$ and $ArH^+$. This agrees well with our measurements of mass spectrum for positive ions (figure 1(b)). The concentrations of $H_2^+$ and $H^+$ are essentially smaller than those of the dominant ions because of their intensive loss in the collisions with argon atoms and acetylene molecules, respectively. It is also due to the fact that the cross-section for ionization of $C_2H_2$ by electrons is larger than those for $H_2$ and $H$ [17].

The densities of $Ar^+$ and $H_2^+$ increase with enlarging particles ($a_d$), while the densities of other ions including $C_2H_2^+$ are decreasing. These variations are mainly caused by the decrease of the electron density and the increase of the effective electron temperature (figure 4).
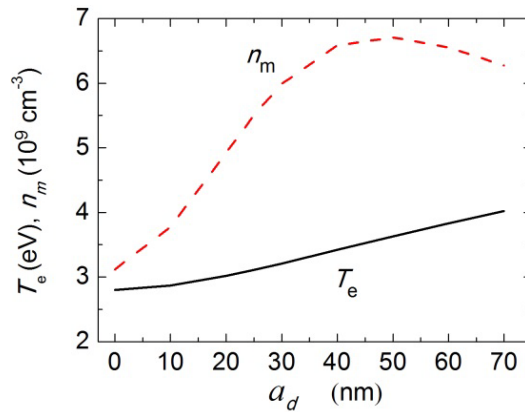


**Figure 4.** $n_m$ and $T_e$ as functions of dust radius. The conditions are the same as in figure 3.

As ground-state Ar atoms have a larger ionization threshold energy than $C_2H_2$ molecules, the increase of $T_e$ favours $Ar^+$ production. Therefore, the $H_2^+$ density increase is mainly due to the enhancement of $H_2^+$ production in collisions of $Ar^+$ with $H_2$. Since the dominant production processes of $C_4H_2^+$ and $C_4H_3^+$ are the collisions of $C_2H_2^+$ with $C_2H_2$, the decrease of the acetylene density with $a_d$ leads to a reduction of the density of these ions.

For the same reasons, the $C_2H_3^+$ production, mainly due to $C_2H_2^+$ - $H_2$ collisions, decreases with $a_d$. The $C_6H_4^+$ density reduces also with $a_d$ because of the decrease of $C_4H_2^+$ and $C_2H_2$ densities ($C_6H_4^+$ is produced by collisions between $C_4H_2^+$ and $C_2H_2$) and due to higher losses of $C_6H_4^+$ on dust particles. The smaller $ArH^+$ density at larger $a_d$ is mainly due to the enhancement of the ion loss on the dust.

The metastable atom density increases with a particle enlargement from $a_d = 0$ to $a_d = 50$ nm and then decreases at larger dust radii. This is caused by an enlargement of $T_e$ and by the $n_e$ decrease, respectively (figure 4).

The concentration of negative ions $C_2H^-$ decreases with growing particle radius due to a reduction of the anion generation by the attachment of electrons to $C_2H_2$ (since $n_e$ decreases), as well as due to an enhancement of the negative ion loss in collisions with $Ar^+$ ions.


*4.2 The afterglow of $C_2H_2$ plasma*

In this subsection, we will analyze how dust particles affect the $C_2H_2$ plasma afterglow. In figure 5, the densities of $C_2H$ and $H$ radicals are shown during dust-free and dusty-plasma afterglows. The density of $C_2H$ decreases more rapidly with time $t$ in the dust-free afterglow comparing with the dusty case. This is due to larger $C_2H_2$ density in the dust-free case (figure 3(a)) and, as a result, more intensive loss of $C_2H$ in collisions with $C_2H_2$ ($C_2H + C_2H_2 \rightarrow C_2H_2 + H$). The decay time for $H$ in dust-free plasma afterglow is nearly the same as that in dusty plasma case because the loss of $H$ in both cases is mainly defined by the diffusion to the walls. In the dusty case, the loss of $H$ on dust particles for small dust radius and density, considered here, is small.
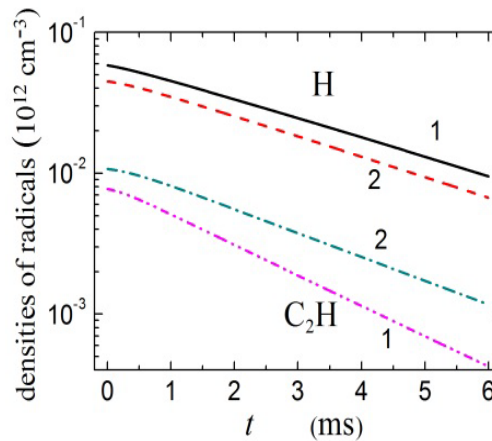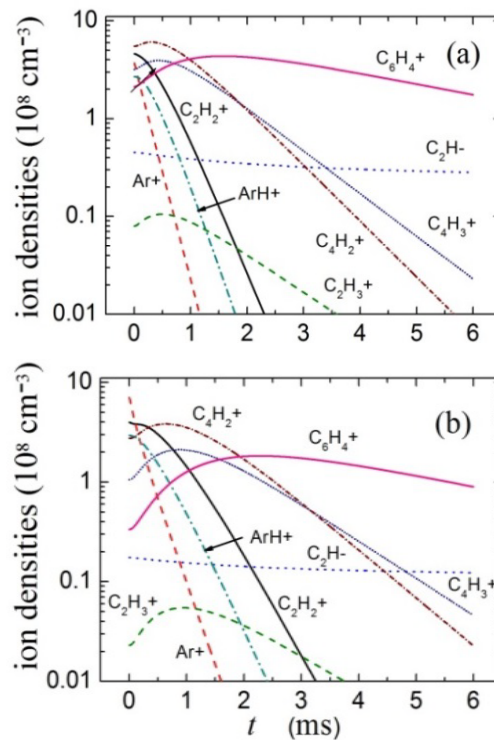


**Figure 5.** Calculated densities of $C_2H$ and $H$ in the dust-free (curves 1) and dusty-plasma (curves 2) afterglows as functions of time. The results are obtained for $a_d$=25 nm, $n_d = 10^7$ cm$^{-3}$. The other external conditions are the same as in figure 3.


The decay times for radical species ($H$ and $C_2H$) are small because the frequencies

characterizing the radical losses (due to the diffusion to the walls and their collisions with nonradical neutrals) are rather large. For example, the frequency characterizing the loss of $C_2H$ in collisions with $C_2H_2$ for $n_{C2H2} = 2\times10^{12}$ cm$^{-3}$ is $2.6\times10^2$ s$^{-1}$, i.e. the decay time is about 4 ms.

In the afterglow, the densities of radical species, ions, metastable argon atoms and electrons are decreasing with time (figures 5 - 7), and, as a result, the density of $C_2H_2$ is increasing because of acetylene injection into the discharge chamber, while the densities of $H_2$ and $C_4H_2$ become smaller because of less intensive generation of these molecules from $C_2H_2$. The time $t_1 = R/n_{C2H2}(0)$, characterizing the $C_2H_2$ density increase in the afterglow is about 0.5 s. Here, it was used: $R = 4.48\times10^{17}Q_{C2H2}/V$, $Q_{C2H2}$=1.11 sccm, $V$ the plasma volume and $n_{C2H2}(0) = 2\times10^{12}$ cm$^{-3}$ the acetylene density in the power on phase.



**Figure 6.** Calculated densities of main ions in the dust-free (a) and dusty-plasma (b) afterglows as functions of time. The conditions are the same as in figure 5.
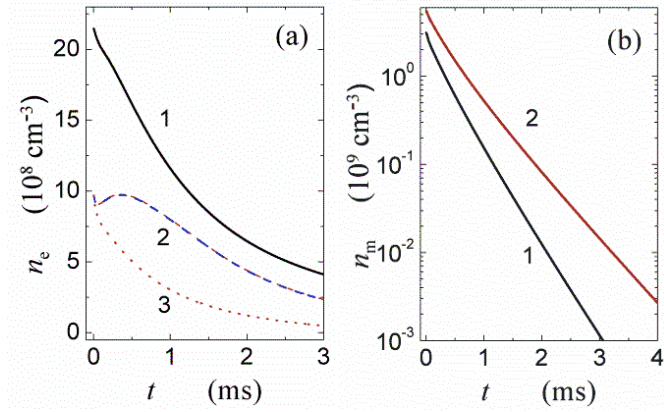
**Figure 7.** (a) $n_e$ as a function of time for the dust-free case (curve 1) and for the dusty-plasma cases when the electron generation in $Ar_m$- $C_2H_2$ collisions is taken into account (curve 2) and neglected (curve 3). (b) The density of $Ar_m$ for the dust-free (curve 1) and dusty-plasma (curve 2) cases accounting for all the collisional processes. The external conditions are the same as in figure 5.

The times characterizing losses of nonradical species, $C_2H_2$, $H_2$ and $C_4H_2$, in which are caused by collisions with radical species, ions, metastable argon atoms and electrons are essentially larger than for radical neutrals because of small frequencies for these collisions. For example, the frequencies and corresponding times characterizing the loss of $C_2H_2$ in collisions with $C_2H$, $Ar^+$ and $Ar_m$ for $n_{C2H} = 10^{10}$ cm$^{-3}$, $n_{Ar}^+ = 10^9$ cm$^{-3}$, $n_m = 5 \times 10^9$ cm$^{-3}$ are, respectively, 1.3, 0.42 and 2.65 s$^{-1}$; 0.77, 2.38 and 0.38 s.

Thus, the densities of nonradical species, $C_2H_2$, $H_2$ and $C_4H_2$, are nearly independent on time for the afterglow times considered here. The long time scales for feeding new $C_2H_2$ molecules and for losses of $C_2H_2$, $H_2$ and $C_4H_2$ explain this stability in the ms range.

The densities of $C_2H_2^+$, $Ar^+$ and $ArH^+$ decrease during the afterglow due to a reduction of the effective electron temperature, $n_e$ and $n_m$ (figure 7). Their main loss mechanism are the collisions with nonradical neutrals, which are having a relatively constant density in the ms time scale. And therefore, the ion losses do not change much in the afterglow. The decay time for $Ar^+$ is smaller than that for other ions because it exclusively produced in electron-neutral collisions, while other ions are also produced in collisions of neutrals with ions and/or metastable atoms.

Diffusion to the walls is one of the main loss processes for $C_2H_3^+$, $C_4H_2^+$, $C_4H_3^+$ and $C_6H_4^+$, and it is strongly reduced in the afterglow because of the decrease of $T_e$. They are predominantly produced in collisions of ions and metastable argon atoms with neutrals. In the beginning of the afterglow, the production dominates over the losses by diffusion, and, therefore, the ion densities increase.

Note also that at large afterglow times ($t > 2$ ms), the density of $C_6H_4^+$ decreases more slowly than for other ions because of the smaller rate of collision with $C_2H_2$ ($7 \times 10^{-11}$ cm$^3$/s) compared to other ions (for example, $1.2 \times 10^{-9}$ cm$^3$/s for $C_2H_2^+$- $C_2H_2$ collisions). Moreover, the decay time due to diffusion to the walls increases with increasing the ion mass due to lower velocities. The

densities of $Ar^+$, $C_2H_2^+$, $ArH^+$, $C_2H_3^+$, $C_4H_2^+$ and $C_4H_3^+$ ions decrease faster in the dust-free case than in the dusty one. In our opinion, this is due to larger densities of $C_2H_2$ and $H_2$ in the former case and, as a result, more intensive loss of these ions in collisions with the molecules.

The density of negative ions decreases more slowly than the one of positive ions. This is due to the model assumption that the anions do not deposit on the plasma walls and to a smaller collision rate with $C_2H_2$ for $C_2H^-$ than for positive ions. The decrease of the anion density at large afterglow times is mainly due to the collisions with hydrogen atoms.

We have also analyzed the time-dependence for $n_e$ in the dust-free and dusty plasma afterglows. One can see in figure 7 that the density of electrons in the dust-free case decreases during the whole afterglow time (curve 1). This is mainly due to electron diffusion to the walls. In the dusty case, the electron density drops at very small afterglow times ($t < 0.05$ ms) and then increases at $0.05$ ms $< t < 0.35$ ms (curve 2).

The time-dependencies for electron density in the dust-free and dusty afterglows are similar to those obtained for argon plasma afterglows [52]. The presence of a peak in the time-dependence for $n_e$ in the case of argon dusty afterglow was explained by the release of free electrons from the dust particles [10] and/or by the electron generation in metastable-metastable collisions [52]. Here, in the Ar/ $C_2H_2$ case, we find, that the electron production in collisions of metastable atoms with acetylene molecules ($Ar_m + C_2H_2 \rightarrow C_2H_2^+ + Ar + e^-$) [13] is responsible for it. To check the latter conclusion, the calculations were carried out without this process leading to curve 3 in figure 7 without any peak. We also carried out the calculations neglecting the electron generation in metastable-metastable collisions, and the effect of this process on the time-dependence of $n_e$ was found to be small.

The metastable density is larger in the dusty-plasma afterglow than that in the dust-free case (figure 7(b)) because of larger effective electron temperature at $t = 0$ in the former case. $n_m$ decreases more slowly in the dusty-plasma afterglow because the metastable losses are mainly due to their collisions with $C_2H_2$, $H_2$ and $C_4H_2$ (the densities of these molecules are larger in the dust-free case). Due to the losses in collisions with neutrals, the metastable density decreases more rapidly in the Ar-$C_2H_2$ plasma afterglow than in the Ar one (please, compare the curves in figure 7 of this paper with the curves in figure 6(a) of [52]), in agreement with experimental results of Stefanovic et al. (figure 8 of [13]).

The dust charge as a function of time in the afterglow was also calculated. It was found that the dependence for $Z_d$ is similar to that in argon dusty afterglow (figure 4(c) in [52]). For the conditions corresponding to curve 2 in figure 7(a), the dust charge at $t = 3$ ms was found to be -5e. Note that the dust charge fluctuation due to the discreteness of the charging process is rather large here [63-65]. In this case, the deviation from the equilibrium dust charge $\delta Z_d$

($\approx |Z_d|^{1/2}\sqrt{(\tau + z)/z(1 + \tau + z)}$ [63], where $\tau = T_i/T_e$, $T_i$ is the ion temperature and $z = e^2|Z_d|/a_dT_e$ or $\delta Z_d \approx 0.5|Z_d|^{1/2}$ [64]) is nearly 1.1. Thus, $\delta Z_d/Z_d \approx 0.22$ for the case considered here. The deviation is smaller in the glow case and increases with increasing the afterglow time and decreasing $a_d$. Therefore, our approach for description of dust charge is approximate for large afterglow times and nanometre-sized particles. Meantime, in [66], it was shown that the time-dependence for electron density in a dusty plasma afterglow calculated using the orbital motion limited theory agrees well with that obtained using the Monte Carlo approach. Note also that our approach for calculation of $Z_d$ does not account for a release of electrons from dust particles by ion bombardment due to field induced emission or by other mechanisms [66]. If the electron emission yield is of the order of 1, the electron release from dust particles may essentially affect plasma properties [52, 66]. Meantime, experiments show that the value of the intrinsic secondary electron yield from carbonaceous dust material is essentially smaller than 1 [66]. Our model for dust charging also assumes that the dust particles are spherical. However, in some experiments the shape of dust particles may be not spherical affecting essentially the collection of electrons and ions by dust particles and the particle motion in the plasma [67, 68].

Therefore, the dust charging model here may be used only for qualitative analysis of the dust charging process in Ar/C$_2$H$_2$ plasmas. For quantitative analysis of the problem, one has to account in the model for the charge discreteness, different secondary emission processes and for nonsphericity of dust particles.

## 5. Summary

In summary, we have analysed by a spatially-averaged model how dust particles affect the properties of glow and afterglow Ar/C$_2$H$_2$ plasmas. For the glow plasma case, it has been shown that the densities of C$_2$H$_2$, H$_2$ and C$_4$H$_2$ molecules at the same external conditions are smaller in the dusty plasma than in the dust-free case due to the enhancement of their losses in various collisional processes. This enhancement is mainly due to the increase of the effective electron temperature caused by collection of electrons on the dust. The temperature increase is accompanied by more intensive production of Ar$^+$ ions and, as a result, by an increase of their density. Meantime, due to enhanced collection of electrons and ions by dust particles, the densities of most hydrocarbon ions reduced at bigger dust radius. Because of the competition between the increase of $T_e$ and the decreasing of $n_e$, the metastable atom density grows with $a_d$ at moderate dust radii (here, $a_d \leq 50$ nm) and decreases at larger dust radii. The dust particles also affect the radical, ion and electron concentrations and the density of metastable argon atoms in the Ar/C$_2$H$_2$ plasma afterglow. Since the density of acetylene molecules is larger in a dust-free plasma than in the dusty one, the densities of C$_2$H radicals, most positive ions and metastable argon atoms

decrease more rapidly in the afterglow as a consequence of their intensified losses in collisions with nonradical neutrals. Due to the larger density of argon metastable atoms in the dusty plasma in turn, the electron production from collisions between metastable atoms and $C_2H_2$ molecules is more intensive leading to a possible peak in the electron density during the afterglow. The model and numerical results presented here are different from those proposed in our earlier studies and the works of previous authors. In particular, our previous numerical results on glow and afterglow dusty plasmas [52, 54] were obtained neglecting chemical processes in plasma volume. While in the earlier works on $Ar/C_2H_2$ and $C_2H_2$ plasmas [16–21] the effects of dust particles on the plasmas have not been considered. The numerical results for glow and afterglow regimes presented here are obtained accounting for main chemical processes in $Ar/C_2H_2$ plasma, as well as the effects of dust particles on plasma properties. The results for the glow regime are compared and found to be in a good qualitative agreement with our recent experimental results on glow $Ar/C_2H_2$ plasma, while the numerical results on the afterglow plasma are in a good qualitative agreement with experimental results from the literature. The presented results are relevant to many applications involving chemically-active plasmas containing impurities, especially gas discharge plasmas used for the synthesis of novel nanomaterials.

## Acknowledgements

## References

## References

[1] *Dusty Plasmas: Physics, Chemistry, and Technological Impacts in Plasma Processing*, edited by A. Bouchoule A 1999 (New York: Wiley)
[2] Vladimirov S V and Ostrikov K 2004 *Phys. Rep.* **393** 175
[3] Winter J 2004 *Plasma Phys. Control. Fusion* **46** B583
[4] Mikikian M, Labidi S, von Wahl E, Lagrange J F, Lecas T, Massereau-Guilbaud V, Géraud-Grenier I, Kovacevic E, Berndt J, Kersten H and Gibert T 2017 *Plasma Phys. Control. Fusion* **59** 014034
[5] Hong S, Berndt J and Winter J 2003 *Plasma Sources Sci. Technol.* **12** 46

[6] Deschenaux Ch, Affolter A, Magni D, Hollenstein Ch and Fayet P 1999 *J. Phys. D: Appl. Phys.* **32** 1876

[7] Benedikt J, Consoli A, Schulze M and von Keudell A 2007 *J. Phys. Chem. A* **111** 10453

[8] Thejaswini H C, Peglow S, Martens U, Sushkov V and Hippler R 2014 *Contrib. Plasma Phys.* **54** 683

[9] Do H T, Thieme G, Frohlich M, Kersten H and Hippler R 2005 *Contrib. Plasma Phys.* **45** 378

[10] Winter J, Berndt J, Hong S H, Kovačević E, Stefanović I and Stepanović O 2009 *Plasma Sources Sci. Technol.* **18** 034010

[11] Herrendorf A P, Sushkov V and Hippler R 2017 *J. Appl. Phys.* **121** 123303

[12] Berndt J, Kovacevic E, Stefanovic I and Boufendi L 2009 *J. Appl. Phys.* **106** 063309

[13] Stefanović I, Sadeghi N, Winter J and Sikimić B 2017 *Plasma Sources Sci. Technol.* **26** 065014

[14] Winter J, Berndt J, Hong S H, Kovačević E, Stefanović I and Stepanović O 2009 *Plasma Sources Sci. Technol.* **18**034010

[15] Stefanović I, Sadeghi N and Winter J 2010 *J. Phys. D: Appl. Phys.***43** 152003

[16] Stoykov S, Eggs C and Kortshagen U 2001 *J. Phys. D: Appl. Phys.* **34** 2160

[17] De Bleecker K, Bogaerts A and Goedheer W 2006 *Phys. Rev. E* **73** 026406

[18] Mao M, Benedikt J, Consoli A and Bogaerts A 2008 *J. Phys. D: Appl. Phys.* **41** 225201

[19] Ariskin D A, Schweigert I V, Alexandrov A L, Bogaerts A and Peeters F M 2009 *J. Appl. Phys.* **105** 063305

[20] Schweigert I V, Alexandrov A L and Ariskin D A 2014 *Plasma Chem. Plasma Process.* **34** 671

[21] Akhoundi A and Foroutan G 2017 *Phys Plasmas* **24** 053516

[22] Consoli A, Benedikt J and von Keudell A 2008 *J. Phys. Chem. A* **112** 11319

[23] Hinz A M, von Wahl E, Faupel F, Strunskus T and Kersten H 2015 *J. Phys. D: Appl. Phys.* **48** 055203

[24] Gudmundsson J T 2001 *Plasma Sources Sci. Technol.* **10** 76

[25] Godyak V A, Piejak R B and Alexandrovich B M 1992 *Plasma Sources Sci. Technol.* **1** 36

[26] Janev R K and Reiter D 2004 *Phys. Plasmas.* **11** 780

[27] Yanguas-Gil A, Cotrino J and Alves L 2005 *J. Phys. D: Appl. Phys.* **38** 1588

[28] Ali M A and Stone P M 2008 *Int. J. Mass Spectrom.* **271** 51

[29] Deutsch H, Becker K, Grum-Grzhimailo A N, Bartschat K, Summers H, Probst M, Matt-Leubner S and Märk T D 2004 *Int. J. Mass Spectrom.* **233** 39

[30] Mityureva A A and Smirnov V V 2004 *Opt. Spektrosk.* **97** 508

[31] Rutrowsky J, Drost H and Spangenber H J 1980 *Ann. Phys.* **492** 259

[32] Shah M B, Elliott D S and Gilbody H B 1987 *J. Phys. B: At. Mol. Phys.* **20** 3501

[33] Yoon J S, Song M Y, Han J M, Hwang S H, ChangW S, Lee B J and Itikawa Y 2008 *J. Phys. Chem. Ref. Data* **37** 913

[34] Barckholtz C, Snow T P and Bierbaum V M 2001 *Astrophys. J.* **547** L171

[35] Gordillo-Vazquez F J and Albella J M 2003 *J. Appl. Phys.* **94** 6085

[36] Sode M, Jacob W, Schwarz-Selinger T and Kersten H 2015 *J. Appl. Phys.* **117** 083303

[37] Hjartarson A T, Thorsteinsson E G and Gudmundsson J T 2010 *Plasma Sources Sci. Technol.* **19** 065008

[38] Knight J S, Freeman C G, McEwan M J, Anicich V G and Huntress Jr W T 1987 *J. Phys. Chem.* **91** 3898

[39] Anicich V and McEwan M 1997 *Planet. Space Sci.* **45** 897

[40] http://www.udfa.net/

[41] Herbst E and Leung C 1989 *Ap. J. Supl. Ser.* **69** 271

[42] Moses J I and Bass S F 2000 *J. Geophys. Res.* **105** 7013

[43] Miasek P G and Beauchamp J L 1979 *In. J. Mass Spectrom. Ion Phys.* **15** 49

[44] McEwan M J, Scott G B I, Adams N G, Babcock L M, Terzieva R and Herbst E 1999 *Astrophys. J.* **513** 287

[45] Denysenko I B, Xu S, Long J D, Rutkevych P P, Azarenkov N A and Ostrikov K 2004 *J. Appl. Phys.* **95** 2713

[46] Thorsteinsson E G and Gudmundsson J T 2009 *Plasma Sources Sci. Technol.* 18 045001

[47] Booth J P and Sadeghi N 1991 *J. Appl. Phys.* **70** 611

[48] Sode M, Schwarz-Selinger T, Jacob W and Kersten H 2014 *J. Appl. Phys.* **116** 013302

[49] Cvelbar U, Mozetič M, Poberaj I, Babič D and Ricard A 2005 *Thin Solid Films* **475** 12

[50] Herrebout D, Bogaerts A, Yan M, Gijbels R, Goedheer W and Dekempeneer E 2001 *J. Appl. Phys.* 90 570

[51] Khrapak S A, Ratynskaia S V, Zobnin A V, Usachev A D, Yaroshenko V V, Thoma M H, Kretschmer M, Hofner H, Morfill G E, Petrov O F and Fortov V E 2005 *Phys. Rev. E* **72** 016406

[52] Denysenko I, Stefanović I, Sikimić B, Winter J, Azarenkov N A and Sadeghi N A 2011 *J. Phys. D: Appl. Phys.* **44** 205

[53] Mcdaniel E W and Mason E A 1973 *The mobility and diffusion of ions in gases* (New York: John Wiley & Sons)

[54] Denysenko I, Yu M Y, Ostrikov K and A. Smolyakov A 2004 *Phys. Rev. E* **70** 046403

[55] Phelps A V and Petrovic Z Lj 1999 *Plasma Sources Sci. Technol.* **8** R21

[56] Hayashi M 1990 Electron collision cross sections determined from beam and swarm data by Boltzmann analysis *Nonequilibrium Processes in Partially Ionized Gases* ed M Capitelli and J N Bardsley (New York: Plenum)

[57] Morgan database, www.lxcat.net

[58] Fite W L and Brackmann R T 1958 *Phys. Rev.* **112** 1151

[59] Denysenko I B, Kersten H and Azarenkov N A 2015 *Phys. Rev. E* **92** 033102

[60] Wegner Th, Hinz A M, Faupel F, Strunskus T, Kersten H and Meichsner J 2016 *Appl. Phys. Lett.* **108** 063108

[61] Mikikian M, Boufendi L, Bouchoule A, Thomas H M, Morfill G E, Nefedov A P, Fortov V E and the PKE-Nefedov Team 2003 *New J. Phys.* **5** 19

[62] Sushkov V, Herrendorf A P and Hippler R 2016 *J. Phys. D: Appl. Phys.* **49** 425201

[63] Morfill G E, Tsytovich V N and Thomas H 2003 *Plasma Phys. Rep.* **29** 1

[64] Cui C and Goree J 1994 *IEEE Trans. Plasma Sci.* **22** 151

[65] Piel A and Melzer A 2002 *Plasma Phys. Control. Fusion* **44** R1

[66] Stefanović I, Berndt J, Marić D, Šamara V, Radmilović-Radjenović M, Petrović Z Lj, Kovačević E and Winter J 2006 *Phys. Rev. E* **74** 024606

[67] Miloch W J, Vladimirov S V, Pécseli H L and Trulsen J 2008 *Phys. Rev. E* **78** 036411

[68] Mahmoodi J, Shukla P K, Tsintsadze N L and Tskhakaya D D 2000 *Phys. Rev. Lett.* **84** 2626